Research Article | Vol. 28, No. 19 / 14 September 2020 / Optics Express 28399
Optics EXPRESS

Spectroscopy and diode-pumped laser operation of transparent Tm:$Lu_3Al_5O_{12}$ ceramics produced by solid-state sintering

Fangxin Yue,[1,2] Pavel Loiko,[3] Mengting Chen,[1,4] Josep Maria Serres,[1] Yicheng Wang,[5] Jiang Li,[6] Liza Basyrova,[7] Elena Dunina,[8] Alexey Kornienko,[8] Liudmila Fomicheva,[9] Shibo Dai,[4] Zhenqiang Chen,[4] Ji Eun Bae,[10] Tae Gwan Park,[10] Fabian Rotermund,[10] Venkatesan Jambunathan,[2] Antonio Lucianetti,[2] Tomas Mocek,[2] Magdalena Aguiló,[1] Francesc Díaz,[1] Uwe Griebner,[5] Valentin Petrov,[5] and Xavier Mateos[1,*]

[1] *Universitat Rovira i Virgili (URV), Física i Cristal·lografia de Materials i Nanomaterials (FiCMA-FiCNA)-EMaS, 43007 Tarragona, Spain*
[2] *HiLASE Centre, Institute of Physics of the Czech Academy of Sciences, Za Radnicí 828, 25241 Dolní Brežany, Czech Republic*
[3] *Centre de Recherche sur les Ions, les Matériaux et la Photonique (CIMAP), UMR 6252 CEA-CNRS-ENSICAEN, Université de Caen Normandie, 6 Boulevard du Maréchal Juin, 14050 Caen Cedex 4, France*
[4] *Department of Optoelectronic Engineering, Jinan University, Guangzhou 510632, China*
[5] *Max Born Institute for Nonlinear Optics and Short Pulse Spectroscopy, Max-Born-Str. 2a, 12489 Berlin, Germany*
[6] *Key Laboratory of Transparent and Opto-Functional Inorganic Materials, Shanghai Institute of Ceramics, Chinese Academy of Sciences, 585 Heshuo, Shanghai 201899, China*
[7] *ITMO University, 49 Kronverkskiy Pr., 197101 St. Petersburg, Russia*
[8] *Vitebsk State Technological University, 72 Moskovskaya Ave., 210035 Vitebsk, Belarus*
[9] *Belarusian State University of Informatics and Radioelectronics, 6 Brovki St., 220027 Minsk, Belarus*
[10] *Department of Physics, KAIST, 291 Daehak-ro, Yuseong-gu, 34141 Daejeon, South Korea*
[*] *xavier.mateos@urv.cat*

Abstract: A transparent Tm:$Lu_3Al_5O_{12}$ ceramic is fabricated by solid-state reactive sintering at 1830 °C for 30 h using commercial α-Al_2O_3 and Lu_2O_3/Tm_2O_3 powders and sintering aids - MgO and TEOS. The ceramic belongs to the cubic system and exhibits a close-packed structure (mean grain size: 21 μm). The in-line transmission at ~1 μm is 82.6%, close to the theoretical limit. The spectroscopic properties of the ceramic are studied in detail. The maximum stimulated-emission cross-section is 2.37×10^{-21} cm^2 at 1749nm and the radiative lifetime of the $^3F_4$ state is about 10 ms. The modified Judd-Ofelt theory accounting for configuration interaction is applied to determine the transition probabilities of Tm^{3+}, yielding the intensity parameters $\Omega_2 = 2.507$, $\Omega_4 = 1.236$, $\Omega_6 = 1.340$ [10^{-20} cm^2] and $\alpha = 0.196\times10^{-4}$ cm. The effect of excited configurations on lower-lying interconnected states with the same J quantum number is discussed. First laser operation is achieved under diode-pumping at 792 nm. A 4 at.% Tm:$Lu_3Al_5O_{12}$ ceramic laser generated 3.12 W at 2022-2035nm with a slope efficiency of 60.2%. The ceramic is promising for multi-watt lasers at >2 μm.

#400802 https://doi.org/10.1364/OE.400802
Journal © 2020 Received 1 Jul 2020; revised 31 Jul 2020; accepted 31 Jul 2020; published 9 Sep 2020

Optics EXPRESS

1. Introduction

Transparent ceramics doped with rare-earth ions (RE^{3+}) represent a promising alternative to the single-crystal development for laser applications [1–3]. Their advantages lie in the technological area, as they offer (i) easier fabrication methods, (ii) lower synthesis temperatures, (iii) size-scalable production, (iv) optical isotropy and (v) the possibility to control the volume of RE^{3+} doping or (vi) to fabricate composite structures [4]. Physically, ceramics may offer compositions which are not present in the single-crystal form and allow for higher RE^{3+} doping levels. When going from a single-crystal to polycrystalline ceramics, the spectroscopic properties of the RE^{3+} ions are typically preserved [5]. A proper fabrication also sustains the thermal and thermo-optical response of the material. As a result, RE^{3+}-doped ceramics are of interest for efficient and power-scalable lasers.

So far, the most widespread material for fabrication of transparent ceramics is the cubic (sp. gr. $Ia\bar{3}d$) yttrium aluminum garnet, $Y_3Al_5O_{12}$. The first studies focused on RE:$Y_3Al_5O_{12}$ transparent ceramics for emission at ~1 μm based on the Nd^{3+} [1–3] and Yb^{3+} [6,7] active dopant ions and, more recently, the interest shifted to the ~2 μm spectral range [8–10]. The 2-μm laser emission is eye-safe and primarily achieved with Tm^{3+} and Ho^{3+} doping. The lasers operating at ~2 μm have multiple applications in remote sensing (LIDAR), wind mapping, spectroscopy, range-finding or medicine. They can also be used for nonlinear frequency conversion into the mid-IR [11]. In particular, the thulium (Tm^{3+}) ion benefits from (i) large Stark splitting of the ground-state ($^3H_6$) leading to broadband emission, (ii) strong absorption at ~0.8 μm (the $^3H_6 \rightarrow {}^3H_4$ transition) allowing for diode-pumping and (iii) an efficient cross-relaxation (CR) process for adjacent Tm^{3+} pairs, $^3H_6 + {}^3H_4 \rightarrow {}^3F_4 + {}^3F_4$, increasing the pump quantum efficiency up to 2 [12]. Tm^{3+}-doped garnets are also known for long upper laser level lifetimes (~10 ms) and emission wavelengths extending beyond 2 μm [13], where the unwanted structured absorption of water in the atmosphere is absent. The latter is in particular relevant for mode-locked (ML) lasers operating at ultrashort pulse durations (broad spectra) with specific applications [14].

Tm:$Y_3Al_5O_{12}$ laser ceramics have been previously demonstrated [8,15–17]. Gao *et al.* reported on a continuous-wave (CW) diode-pumped Tm:$Y_3Al_5O_{12}$ ceramic laser delivering 6.05 W at 2016nm with a slope efficiency of 65% [17]. Gluth *et al.* demonstrated a Tm:$Y_3Al_5O_{12}$ ceramic oscillator ML by a GaSb-based SEmiconductor Saturable Absorber Mirror (SESAM) delivering 3-ps pulses at 2012nm at a repetition rate of 89 MHz [18].

Another compound in the cubic garnet family, i.e., lutetium aluminum garnet, $Lu_3Al_5O_{12}$, is known for its better thermal properties as compared to its yttrium counterpart which is advantageous for the ceramic technology [19,20]. Considering Tm^{3+} doping, $Lu_3Al_5O_{12}$ is attractive because of the closeness of the ionic radii of Tm^{3+} and Lu^{3+} (as compared to Y^{3+}). Studies on Tm:$Lu_3Al_5O_{12}$ single-crystals exist [21,22], however, there is a lack of information about such ceramics. Wang *et al.* reported on a ML Tm:$Lu_3Al_5O_{12}$ ceramic laser delivering 2.7 ps pulses at 2022nm; a broad tuning range of 1808-2088nm was also demonstrated [23]. Zhou *et al.* reported on a CW Tm:$Lu_3Al_5O_{12}$ ceramic laser delivering an output power of 2.64 W at 2016nm with a slope efficiency of only 35.6% [24]. Note that $Lu_3Al_5O_{12}$ ceramics doped with other RE^{3+} ions are also known [25,26].

In the present work, we demonstrate the potential of Tm:$Lu_3Al_5O_{12}$ transparent ceramics for highly-efficient multi-watt laser operation at ~2 μm and study thoroughly their spectroscopic properties, which are of key importance for the development of CW and in particular ML lasers.

2. Synthesis of ceramics

Tm:$Lu_3Al_5O_{12}$ transparent ceramics were prepared by solid-state reactive sintering of commercial α-Al_2O_3 (purity: 99.98%) and Lu_2O_3/Tm_2O_3 (5N) powders, using MgO (5N) and tetraethoxysilane (TEOS, 5N) as sintering aids [23]. The raw materials were mixed in a stoichiometric

Optics EXPRESS

ratio of $(Lu_{0.96}Tm_{0.04})_3Al_5O_{12}$ and ball milled for 12 h with absolute ethyl alcohol as milling medium. Afterwards, we dried the slurry for 2 h at 80 °C in an oven, grounded and sieved it subsequently through a 200-mesh screen. Finally, we calcined it at 800 °C for 1 h to remove organic components. After the preparation, we pressed uniaxially the powders into pellets (diameter: 20 mm) at 50 MPa and cold isostatically pressed (CIP) at 250 MPa. The green-bodies were sintered at 1830 °C for 30 h in a tungsten mesh-heated vacuum furnace. In order to remove the oxygen vacancies, we annealed the samples at 1450 °C for 10 h in air. The Tm^{3+} doping level of 4.0 at.% corresponds to $N_{Tm} = 5.65\times10^{20}$ cm^{-3} (calculated using a density ρ_{calc} of 6.695 g/cm^3 determined from the XRD data).

The ceramics were transparent and colorless, as shown in Fig. 1. For spectroscopic studies, a sample with a thickness t of 3.08 mm was cut and both surfaces were polished to laser-grade quality.

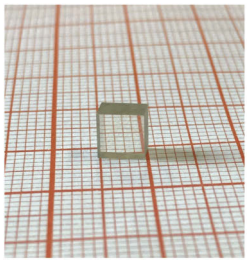

Fig. 1. Photograph of a laser-grade-polished Tm:$Lu_3Al_5O_{12}$ transparent ceramic sample.

3. Characterization of the fabricated ceramics

3.1. Structure and morphology

The structure and phase purity of the fabricated transparent ceramics were confirmed by X-ray diffraction (XRD), see Fig. 2(a). The ceramic sample was finely powdered for the XRD study. The ceramic has a cubic structure similar to that of undoped $Lu_3Al_5O_{12}$ (ICSD card #23846, sp. gr. $Ia\bar{3}d - O^{10}_h$, No. 230) [27]. No traces of other phases are observed in the XRD pattern. The lattice constant is $a = 11.91$ Å. It is slightly larger than that of undoped $Lu_3Al_5O_{12}$ ($a = 11.90$ Å). Tm^{3+} ions substitute for the Lu^{3+} ones in a single type of sites (D_2 symmetry) [28]. The difference in ionic radii of Tm^{3+} (0.994 Å) and Lu^{3+} (0.977 Å) for VIII-fold coordination by O^{2-} [29] explains the observed lattice expansion.

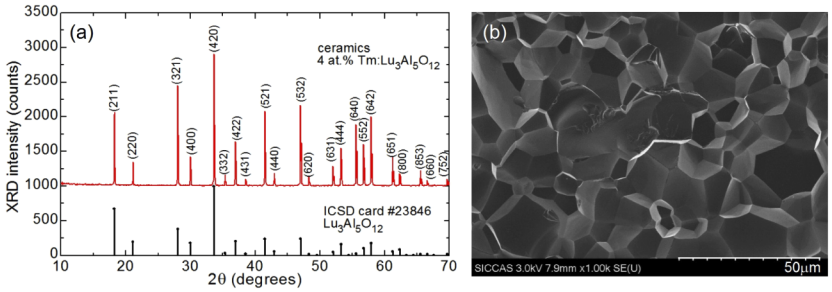

Fig. 2. Structure and microstructure of the Tm:$Lu_3Al_5O_{12}$ ceramic: (a) X-ray powder diffraction (XRD) pattern, *black peaks* stand for undoped $Lu_3Al_5O_{12}$ (ICSD card #23846), *numbers* denote the Miller's indices (*hkl*); (b) Field-Emission Scanning Electron Microscope (FESEM) image of a fractured surface, the scale bar is 50 μm.

Optics EXPRESS

The study of the microstructure by Field-Emission Scanning Electron Microscopy (FESEM), Fig. 2(b), reveals a close-packed structure with clean grain boundaries and lack of pores. The grain size distribution was analyzed using the ImageJ software counting >50 grains. The measured grain sizes were multiplied by the shape factor of 1.2. The mean grain size is 21 ± 4 μm.

3.2. Raman spectroscopy

The vibronic properties of the fabricated ceramic were studied with Raman spectroscopy, see Fig. 3, showing an unpolarized Raman spectrum for an excitation wavelength of 514 nm. For cubic $Lu_3Al_5O_{12}$ containing 80 atoms in the unit-cell, the factor-group analysis predicts 97 lattice modes. They are characterized (at $\boldsymbol{k} = 0$, the center of the Brillouin zone) by the following set of irreducible representations [30]: $\Gamma = 3A_{1g} + 8E_g + 14F_{2g} + 5A_{1u} + 5A_{2u} + 5A_{2g} + 10E_u + 14F_{1g} + 16F_{2u} + 17F_{1u}$. Here, 25 lattice modes (A_{1g}, E_g and F_{2g}) are Raman-active. In Fig. 3, 14 bands are observed and assigned to the lattice vibrations.

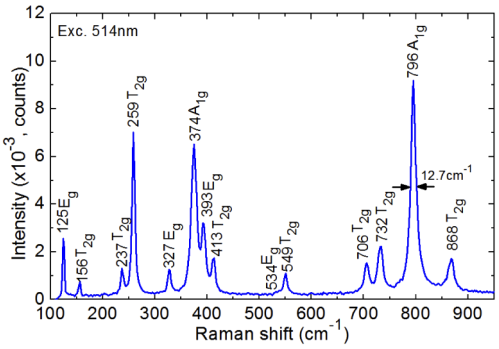

Fig. 3. Unpolarized Raman spectrum of the Tm:$Lu_3Al_5O_{12}$ ceramic; *numbers* indicate Raman frequencies in cm^{-1}.

The most intense Raman band at 796 cm^{-1} (A_{1g}) is due to the breathing mode of the [AlO_4] tetrahedron [31]. Its full width at half maximum (FWHM) is 12.7 cm^{-1}. Other intense bands appear at lower frequencies, at 259 cm^{-1} (T_{2g}) and 374 cm^{-1} (A_{1g}). The maximum phonon energy $h\nu_{ph}$ for the studied ceramic is 868 cm^{-1} (T_{2g}).

3.3. Optical absorption spectroscopy

The transmission spectrum of the ceramic is shown in Fig. 4. At 1.0 μm (out of the absorption of Tm^{3+} ions), the transmission T amounts to 82.6% which is close to the theoretical value set by the Fresnel losses, $T_0 = 83.6\%$ (assuming a refractive index $n = 1.826$ [32]). This value confirms the very good optical quality of the fabricated ceramic.

The absorption bands are due to Tm^{3+} transitions from the ground-state ($^3H_6$) to the excited-states (from $^3F_4$ to $^1D_2$). The absorption cross-sections were calculated from the absorption coefficient α_{abs} according to the equation $\sigma_{abs} = \alpha_{abs}/N_{Tm}$. The α_{abs} values, in their turn, were determined from the transmission spectrum, cf. Figure 4, as $\alpha_{abs} = -\ln(T/T_0)/t$ [cm^{-1}] where the thickness t is expressed in cm. For the $^3H_6 \rightarrow {}^3H_4$ transition which is used for conventional pumping of Tm lasers, Fig. 5(a), the maximum σ_{abs} is 5.0×10^{-21} cm^2 at 787.6 nm and the FWHM of several closely located absorption peaks is 12.4 nm. For the $^3H_6 \rightarrow {}^3F_4$ transition, which is spectrally overlapping the ~2 μm emission of Tm lasers, σ_{abs} is 9.5×10^{-21} cm^2 at 1631.9 nm, see Fig. 5(b). In the range of the laser emission (2.02 μm), the reabsorption losses σ_{abs} are $< 0.04\times10^{-21}$ cm^2.

Optics EXPRESS

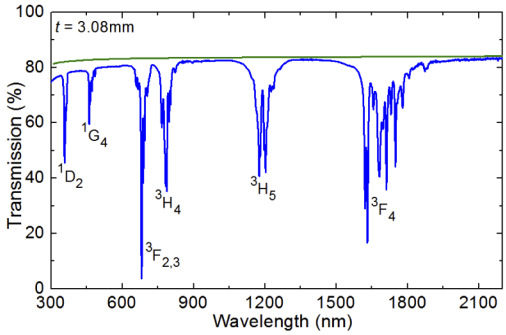

Fig. 4. Transmission spectrum of a laser-grade-polished 4 at.% Tm:$Lu_3Al_5O_{12}$ ceramic sample ($t = 3.08$ mm), *green curve* - theoretical transmission determined by Fresnel reflections.

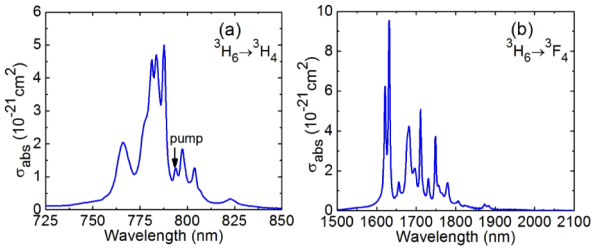

Fig. 5. Absorption cross-section, σ_{abs}, of Tm^{3+} in the $Lu_3Al_5O_{12}$ ceramic for (a) the $^3H_6 \rightarrow {}^3H_4$ transition and (b) the $^3H_6 \rightarrow {}^3F_4$ transition. *Arrow* in (a) indicates the pump wavelength.

3.4. Optical emission spectroscopy

The stimulated-emission (SE) cross-sections, σ_{SE}, for the $^3F_4 \rightarrow {}^3H_6$ transition of Tm^{3+} are shown in Fig. 6(a). They was calculated using a combination of the reciprocity method (RM) [33] and the Füchtbauer-Ladenburg (F-L) equation [34]:

$$\sigma_{SE}(\lambda) = \sigma_{abs}(\lambda)\frac{Z_1}{Z_2}\exp\left(-\frac{hc/\lambda - E_{ZPL}}{kT}\right), \tag{1a}$$

$$\sigma_{SE}(\lambda) = \frac{\lambda^5}{8\pi\langle n\rangle^2\tau_{rad}c}\frac{W(\lambda)}{\int \lambda W(\lambda)\mathrm{d}\lambda}. \tag{1b}$$

In Eq. (1a), Z_m are the partition functions of the lower ($m = 1$) and upper ($m = 2$) manifolds, calculated to be 3.209 and 1.810, respectively ($Z_1/Z_2 = 1.773$), h is the Planck constant, c is the speed of light, λ is the wavelength, k is the Boltzmann constant, T is the temperature (293 K) and $E_{ZPL} = 5527\ \mathrm{cm}^{-1}$ (where ZPL stands for the zero-phonon line) is the energy of the transition between the lowest Stark sub-levels of two multiplets. Here, the values of the partition functions and the ZPL energy [35] are based on the crystal-field calculations, see Section 3.5. In Eq. (1b), $\langle n\rangle = 1.813$ is the refractive index of $Lu_3Al_5O_{12}$ (calculated using the Sellmeier equation [32]) at a mean Tm^{3+} emission wavelength of $\langle\lambda\rangle = 1815$nm (determined in the present work), τ_{rad} is the radiative lifetime of the emitting state ($^3F_4$) and $W(\lambda)$ is the luminescence spectrum.

The simultaneous use of the two methods allows one to avoid the detrimental effect of reabsorption on the measured $W(\lambda)$ spectrum and to quantify σ_{SE} at long wavelengths where the RM gives high error due to the exponential term in Eq. (1a). A reasonable agreement between

Optics EXPRESS

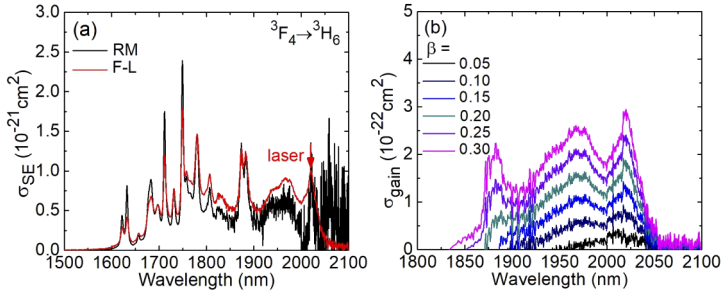

Fig. 6. Stimulated-emission (SE) of Tm^{3+}-doped $Lu_3Al_5O_{12}$ ceramic at ~2 μm ($^3F_4 \rightarrow {}^3H_6$ transition): (a) SE cross-sections, σ_{SE}, calculated using the RM and the F-L equation, and (b) gain cross-section, σ_{gain}, for various inversion ratios β, calculated using a combined SE cross-section spectrum (see the details in the text). *Arrow* in (a) indicates the laser wavelength.

the two methods is observed for $\tau_{rad} = 9.8 \pm 0.3$ ms. To construct the combined SE cross-section spectrum further used for the gain calculations, we have selected the wavelength of 1.88 μm as a borderline. At shorter wavelength, the RM was applied owing to the notable reabsorption and at longer wavelength, we used the F-L equation.

Tm:$Lu_3Al_5O_{12}$ features a broad emission spanning from 1.61 to 2.06 μm. The maximum σ_{SE} is 2.37×10^{-21} cm^2 at 1749nm (as calculated using the RM). In the long-wavelength spectral range where the laser operation is expected, σ_{SE} is lower, namely, 1.03×10^{-21} cm^2 at 2021 nm (the value obtained from the F-L equation).

The $^3F_4 \rightarrow {}^3H_6$ Tm^{3+} lasers operate in a quasi-three-level scheme (exhibiting reabsorption). Thus, the gain at a distinct laser wavelength is quantified as $\sigma_{gain} = \sigma_{SE} - (1 - \beta)\sigma_{abs}$, where $\beta = N_2(^3F_4)/N_{Tm}$ is the inversion ratio, Fig. 6(b). Physically, an increase of β indicates an increased level of losses in the laser (e.g., high output-coupling) according to the rule "gain equals the losses". The evolution of the gain spectra with β explains the variation of the laser wavelength when increasing the output coupling ratio. For Tm:$Lu_3Al_5O_{12}$, a broad peak at ~2020nm dominates in the spectra up to at least $\beta = 0.30$.

The luminescence decay curve measured at 1950nm (emitting state: $^3F_4$) is shown in Fig. 7. It is single-exponential in agreement with a single type of sites for Tm^{3+} ions. The luminescence lifetime $\tau_{lum} = 9.68$ ms is close to the estimated τ_{rad} value (9.8 ± 0.3 ms) which indicates weak non-radiative relaxation and quenching of luminescence from the $^3F_4$ state in the ceramic.

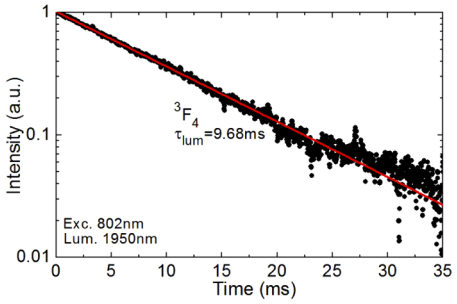

Fig. 7. Luminescence decay curve for the 4.0 at.% Tm:$Lu_3Al_5O_{12}$ ceramic: *symbols* – experimental data; *red line* – single-exponential fit for the luminescence lifetime τ_{lum}.

Optics EXPRESS

3.5. Judd-Ofelt analysis

To assign the transitions in the absorption spectra, we calculated the Stark splitting for the Tm^{3+} multiplets in $Lu_3Al_5O_{12}$ using crystal-field parameters reported for bulk crystals [35]. The D_2 group has four one-dimensional irreducible representations Γ_i ($i = 1, 2, 3, 4$) and each $^{2S+1}L_J$ multiplet is split into $2J + 1$ singlet Stark components. The energy-level scheme is shown in Fig. 8(a). The energies of the Stark sub-levels for all multiplets from $^3H_6$ up to $^3P_2$ are also listed in Table 1 (previously reported only for the upper and lower laser levels).

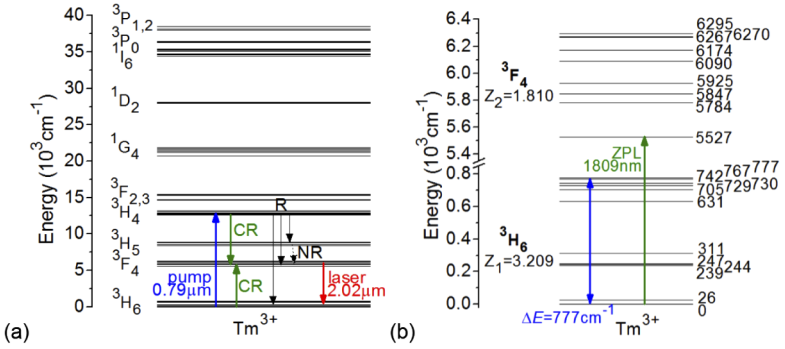

Fig. 8. Energy-level schemes of Tm^{3+}:$Lu_3Al_5O_{12}$: (a) energy-level scheme showing the pump and laser transitions, cross-relaxation (CR), radiative (R) and non-radiative (NR) decays; (b) details of the splitting of the upper and lower laser multiplets; *green arrow* – ZPL transition. The position of the Stark sub-levels is calculated using the crystal-field parameters from [35].

Table 1. Calculated Stark Splitting of Tm^{3+} Multiplets in $Lu_3Al_5O_{12}$

$^{2S+1}L_J$	E, cm^{-1}
$^3H_6$	0, 26, 239, 244, 247, 312, 630, 705, 729, 730, 743, 767, 777
$^3F_4$	5527, 5784, 5847, 5925, 6089, 6174, 6267, 6270, 6295
$^3H_5$	8374,8385, 8542,8561, 8584, 8586, 8813, 8833, 8868, 8889,8897
$^3H_4$	12652, 12677, 12777, 12791, 12830, 12987, 13159, 13160, 13186
$^3F_3$	14673, 14702, 14720, 14753, 14762, 14766, 14766
$^3F_2$	15259, 15293, 15340, 15442, 15463
$^1G_4$	20757, 21205, 21221, 21404, 21541, 21736, 21854, 21883, 21884
$^1D_2$	27954, 27996, 28045, 28055, 28078
$^1I_6$	34426, 34436, 34438, 34468, 34584, 34677, 34740, 35092, 35092, 35279, 35308, 35387, 35399
$^3P_0$	35431
$^3P_1$	36343, 36390, 36464
$^3P_2$	38009, 38035, 38181, 38450, 38505

The details for the $^3H_6$ and $^3F_4$ multiplets are shown in Fig. 8(b). The total splitting of the ground-state ($^3H_6$) is rather large ($\Delta E = 777\ cm^{-1}$) defining a possible emission above 2 μm.

The 4f-4f transition intensities of Tm^{3+}:$Lu_3Al_5O_{12}$ were analyzed using the Judd-Ofelt (J-O) theory [36,37]. The squared reduced matrix elements $U^{(k)}$ in absorption and emission were taken from Ref. [38]. The magnetic-dipole (MD) contributions for J → J' transitions with $\Delta J = 0, \pm 1$ were calculated separately within the Russell-Saunders approximation on wave functions of the

Optics EXPRESS

Tm^{3+} ion under the assumption of a free-ion. More details about the calculation procedure for Tm^{3+} can be found elsewhere [39].

The standard J-O theory and its modification (denoted as the modified Judd-Ofelt (mJ-O) theory) [40,41] accounting for configuration interaction were used. For both approaches, the electric-dipole (ED) line strengths for a J → J' transition can be written as:

$$S^{ED}_{calc}(JJ') = \sum_{k=2,4,6} U^{(k)}\Omega_k. \quad (2)$$

Here, Ω_k ($k = 2, 4, 6$) are the J-O (intensity) parameters. For the standard J-O theory (no configuration interaction), they are constant. In the mJ-O theory, it is assumed that solely the excited configuration with an opposite parity $4f^{n-1}5d^1$ contributes to the configuration interaction, so that the J-O parameters are linear functions of the energies of the two multiplets (E_J and $E_{J'}$) involved in the transition:

$$\tilde{\Omega}_k = \Omega_k[1 + 2\alpha(E_J + E_{J'} - 2E^0_f)]. \quad (3)$$

Here, $E^f{}_0$ is the mean energy of the $4f^n$ configuration and $\alpha \approx 1/(2\Delta)$, where Δ is associated with the energy of the excited-configuration. In particular, if $\Delta \to \infty$, $\Omega_k = constant$ (the standard J-O theory).

The absorption oscillator strengths were determined from the measured absorption spectra (f^{Σ}_{exp}) and calculated using the J-O and mJ-O theories (f^{Σ}_{calc}), as shown in Table 2. Here, the "Σ" superscript stands for the total (ED + MD) value. The latter approach gives much lower root mean square (rms) deviation between f^{Σ}_{exp} and f^{Σ}_{calc}. The corresponding set of parameters - (Ω_k) for the J-O theory and (Ω_k and α) for the mJ-O one are given in Table 3.

Table 2. Experimental and Calculated Absorption Oscillator Strengths[a] for Tm:$Lu_3Al_5O_{12}$ Ceramic

Transition $^3H_6 \to {}^{2S+1}L_J$	$\langle E\rangle_{exp}$,cm^{-1}	n	$f^{\Sigma}_{exp}\times10^6$	$f^{\Sigma}_{calc}\times10^6$ (model[b])		
				J-O	mJ-O	mJ-O[c]
$^3F_4$	5831	1.815	1.45	1.672^{ED}	1.381^{ED}	*0.907^{ED}*
$^3H_5$	8363	1.822	1.41	1.228^{ED} + 0.505^{MD}	1.078^{ED} + 0.505^{MD}	0.875^{ED} + 0.505^{MD}
$^3H_4$	12699	1.831	1.94	1.681^{ED}	1.971^{ED}	1.952^{ED}
$^3F_{2,3}$	14529	1.836	2.93	2.948^{ED}	2.868^{ED}	2.926^{ED}
$^1G_4$	21229	1.857	0.76	0.586^{ED}	0.713^{ED}	0.730^{ED}
$^1D_2$	27871	1.884	2.62	2.506^{ED}	2.644^{ED}	2.626^{ED}
rms dev.				*0.257*	*0.119*	*0.026*

[a] $\langle E\rangle$ - experimental energy barycenter of the multiplet, n - refractive index, f^{Σ}_{exp} and f^{Σ}_{calc} – experimental and calculated absorption oscillator strengths (ED + MD), respectively. ED and MD stand for electric-dipole and magnetic-dipole transitions, respectively.
[b] J-O – "standard" Judd-Ofelt model; mJ-O – modified Judd-Ofelt model.
[c] Varied oscillator strength of the $^3H_6 \to {}^3F_4$ transition.

A direct application of both J-O and mJ-O theories for the description of the transitions (emission) gives a notably underestimated radiative lifetime of the lower-lying excited state ($^3F_4$), namely, $\tau_{rad} = 5.60$ ms (J-O) and 6.78 ms (mJ-O). This is a known problem for Tm^{3+}-doped cubic garnets [42].

To support further considerations, we calculated the wave functions of the Tm^{3+} multiplets with the same total angular momentum quantum number $J = 4$, namely, $^3F_4$, $^3H_4$ and $^1G_4$, see Table 4. Due to the strong spin-orbit interaction, they form a group of strongly interconnected states [45]. Indeed, the non-diagonal elements in Table 4 are comparable in magnitude to the

Optics EXPRESS

Table 3. Parameters of the "Standard" and Modified Judd-Ofelt Theories for Thulium Ions in Various Ceramic Materials

Parameter	$Tm:Lu_3Al_5O_{12}$			$Tm:Y_3Al_5O_{12}$	$Tm:(Lu,Sc)_2O_3$
	This work			[43]	[44]
	J-O	mJ-O	mJ-O[a]	J-O	J-O
$\Omega_2\times10^{20}$, cm^2	1.025	2.164	2.507	0.444	2.429
$\Omega_4\times10^{20}$, cm^2	1.781	1.511	1.236	1.340	1.078
$\Omega_6\times10^{20}$, cm^2	0.799	1.039	1.340	0.674	0.653
$\alpha\times10^4$, cm	–	0.113	0.196	–	–

[a]Varied oscillator strength of the $^3H_6\rightarrow{}^3F_4$ transition.

diagonal ones. Thus, through the $^1G_4$ excited-state of the $4f^n$ configuration, the effect of excited configurations (e.g., $4f^{n-1}5d^1$) is transferred to the lower-lying states, $^3F_4$ and $^3H_4$. In a recent paper [46], this effect was described in terms of the hypersensitivity of the $^3H_6 \rightarrow {}^3F_4$ Tm^{3+} transition to the local ligand field.

Table 4. Wave Functions of Tm^{3+} Multiplets with J = 4 in $Lu_3Al_5O_{12}$

Multiplet [main contribution]	Energy $\langle E\rangle_{calc}$, cm^{-1}	Coefficients of wave function for the $^{2S+1}L_J$ terms		
		$^3F_4$	$^3H_4$	$^1G_4$
$[^3F_4]$	5538	0.7868	−0.2851	0.5474
$[^3H_4]$	12475	0.5300	0.7666	−0.3626
$[^1G_4]$	21025	−0.3162	0.5754	0.7542

To avoid this problem, the mJ-O theory was applied to all the observed Tm^{3+} transitions except $^3H_6 \rightarrow {}^3F_4$ to minimize the rms deviation between f^{Σ}_{exp} and f^{Σ}_{calc}. The results are shown in Table 2 (the last column) following the same calculation procedure as described above. The corresponding intensity parameters are $\Omega_2 = 2.507$, $\Omega_4 = 1.236$, $\Omega_6 = 1.340$ [10^{-20} cm^2] and $\alpha = 0.196\times10^{-4}$ cm (or $\Delta = 25510$ cm^{-1}).

In Table 3, we also provide for comparison the intensity parameters reported for other Tm^{3+}-doped transparent ceramics, i.e., $Tm:Y_3Al_5O_{12}$ [43] and $Tm:(Lu,Sc)_2O_3$ [44].

By using such intensity parameters, we calculated the probabilities of spontaneous radiative transitions $A_{\Sigma}{}^{calc}$, the luminescence branching ratios $B(JJ')$ and the radiative lifetimes of the excited-states τ_{rad} for Tm^{3+} in $Lu_3Al_5O_{12}$ ceramic, see Table 5. Such an approach gives good agreement between the radiative lifetime of the $^3F_4$ state calculated with the mJ-O theory ($\tau_{rad} = 10.32$ ms), its estimation from the calculation of the SE cross-sections by the RM and F-L methods ($\tau_{rad} = 9.8 \pm 0.3$ ms), and the reabsorption-free luminescence lifetime ($\tau_{lum} = 9.68$ ms), see Section 3.4.

Optics EXPRESS

Table 5. Probabilities of the Radiative Spontaneous Transitions[a] for Tm:$Lu_3Al_5O_{12}$ Ceramic

Excited state	Terminal state	$\langle\lambda\rangle$, nm	$A_\Sigma^{calc}(JJ')$, s^{-1}	$B(JJ')$, %	A_{tot}, s^{-1}	τ_{rad}, ms
$^3F_4$	$^3H_6$	1715	96.9^{ED}	100	96.9	10.32
$^3H_5$	$^3F_4$	3949	$7.1^{ED} + 0.2^{MD}$	2.9	255.5	3.91
	$^3H_6$	1196	$157.4^{ED} + 90.8^{MD}$	97.1		
$^3H_4$	$^3H_5$	2306	$23.9^{ED} + 9.1^{MD}$	2.9	1147.3	0.87
	$^3F_4$	1456	$102.5^{ED} + 22.5^{MD}$	10.9		
	$^3H_6$	787	989.3^{ED}	86.2		
$^3F_2+^3F_3$	$^3H_4$	5464	$12.2^{ED} + 0.3^{MD}$	0.3	3910.3	0.26
	$^3H_5$	1622	550.7^{ED}	14.1		
	$^3F_4$	1150	$585.4^{ED} + 63.6^{MD}$	16.6		
	$^3H_6$	688	2698.1^{ED}	69.0		
$^1G_4$	$^3F_2+^3F_3$	1493	$143.5^{ED} + 3.5^{MD}$	4.5	3190.0	0.31
	$^3H_4$	1172	$385.9^{ED} + 33.4^{MD}$	13.2		
	$^3H_5$	777	$1180.8^{ED} + 134.5^{MD}$	41.2		
	$^3F_4$	649	$264.3^{ED} + 10.0^{MD}$	8.6		
	$^3H_6$	471	1034.1^{ED}	32.5		

[a] $\langle\lambda\rangle$ - calculated mean emission wavelength, A^{Σ}_{calc} – probability of radiative spontaneous transitions (ED + MD), B(JJ') – luminescence branching ratio, A_{tot} and τ_{rad} – total probability of radiative spontaneous transitions (ED + MD) and radiative lifetime of the excited state, respectively. ED and MD stand for electric-dipole and magnetic-dipole transitions, respectively.

4. Laser operation

4.1. Laser setup

Laser operation was achieved in a compact plano-plano (microchip-type) cavity, as shown in Fig. 9(a). It was formed by a flat pump mirror (PM) coated for high transmission (HT) at ~0.79 μm and for high reflection (HR) at 1.80–2.08 μm, and a set of flat output couplers (OCs) with a transmission T_{OC} = 1.5%–20% at the laser wavelength of ~2.02 μm. The ceramic laser element (t = 3.08 mm, aperture: 5×5 mm^2) was kept uncoated. It was mounted in a Cu-holder using In foil for better thermal contact from all four lateral sides. The holder was cooled down to 12 °C by circulating water. Both the PM and OC were placed as close as possible to the laser element resulting in a geometrical cavity length of ~3.1 mm.

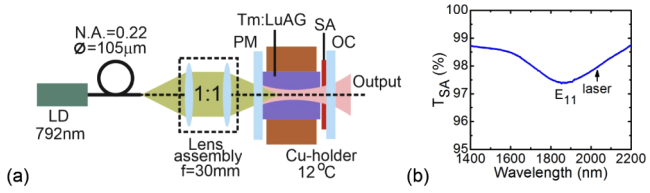

Fig. 9. (a) Scheme of the diode-pumped Tm:$Lu_3Al_5O_{12}$ (Tm:LuAG) ceramic laser: LD – laser diode, PM – pump mirror, OC – output coupler, SA – saturable absorber; (b) transmission spectrum of the SWCNT-SA (Fresnel losses are subtracted).

As a pump source, we used a fiber-coupled (core diameter: 105 μm, N.A. = 0.22) AlGaAs laser diode (MTLC00031, BWT Beijing Ltd.) emitting up to 30 W of unpolarized output at 792 nm ($^3H_6 \rightarrow {}^3H_4$ transition of Tm^{3+}, conventional pumping). Its emission bandwidth was 4.4 nm. The pump radiation was reimaged into the laser element through the PM by a lens assembly

Optics EXPRESS

(1:1 reimaging ratio, focal length f = 30 mm). The OCs were partially reflective at the pump wavelength ($R \approx 40\%$), so that the pumping was in double-pass and the total pump absorption at the laser threshold $\eta_{abs(2-pass)}$ amounted to 33.1 ± 0.5%. The waist of the pump beam in the focus was $2w_P \approx 100$ µm.

For passive Q-switching, a transmission-type saturable absorber (SA) was inserted between the laser element and the OC at a minimum separation. It was based on purified arc-discharge single-walled carbon nanotubes (SWCNTs) [47]. The SWCNT/PMMA composite film (thickness: ~300 nm) was spin-coated onto an uncoated 1-mm-thick glass substrate. In the small-signal transmission spectrum of the SA, Fig. 9(b), a broad absorption band spanning from 1.6 to 2.2 µm is observed. It is assigned to the first fundamental transition of semiconducting nanotubes (E_{11}) with varying tube diameters between 1.5 and 2.2 nm. At the laser wavelength of ~2.02 µm, the internal small-signal transmission (corrected for the Fresnel losses) T_{SA} was 97.9%. According to our previous studies, the saturation intensity of a similar SWCNT-based SA I_{sat} was 7 ± 1 MW/cm^2, the fraction of the saturable losses $\alpha'_S/\alpha'_{SA} = 0.21$ (where $\alpha'_{SA} = 1 - T_{SA}$), both specified for ns pulse durations [10], and the recovery times of the initial absorption are $\tau_{rec} = 0.25$ and 1.16 ps for "fast" and "slow" components, respectively, as determined in a pump-probe experiment [48].

4.2. Continuous-wave laser operation

Continuous-wave laser operation was realized without the SA in the cavity. The input-output power characteristics are shown in Fig. 10(a). The maximum output power reached 3.12 W at 2022-2035 nm with a slope efficiency η of 60.2% (*vs.* the absorbed pump power, P_{abs}). The laser threshold was at $P_{abs} = 0.25$ W and the optical-to-optical efficiency η_{opt} was 18.8% (*vs.* the pump power incident on the crystal). These characteristics were measured for $T_{OC} = 5\%$. Using $T_{OC} >$ 10%, the output deteriorated probably due to increased upconversion losses and energy-migration to impurities associated with high inversion in the gain medium. Although such effects do not affect the slope efficiency directly, they cause stronger heat loading. For low output coupling ($T_{OC} \leq 5\%$), a thermal roll-over was observed for $P_{abs} > 5.5$ W. The power scaling was limited to avoid fracture of the ceramic sample. The laser operated at the fundamental transverse mode, see the inset in Fig. 10(a).

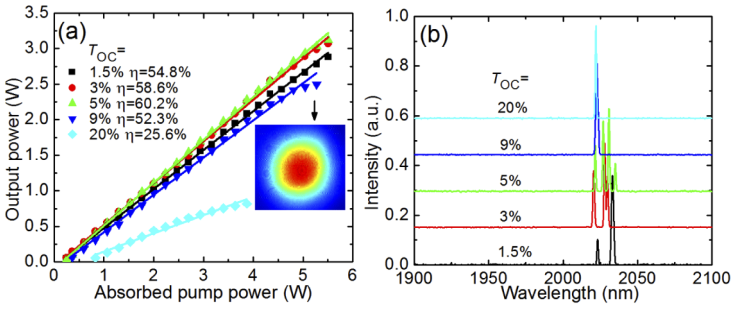

Fig. 10. Continuous-wave (CW) diode-pumped Tm:$Lu_3Al_5O_{12}$ ceramic laser: (a) input-output dependences, η – slope efficiency, *inset* – spatial profile of the laser beam ($T_{OC} = 5\%$, $P_{abs} = 5.3$ W); (b) typical laser emission spectra measured at $P_{abs} = 3.0$ W.

The laser output was unpolarized. The laser emission spectra are shown in Fig. 10(b). They are only weakly dependent on the output coupling, the emission occurred at ~2.02 µm in agreement with the gain spectra, cf. Figure 6(b).

Optics EXPRESS

4.3. Passive Q-switching

Q-switching was realized by inserting the SWCNT-SA into the cavity. There existed an upper limit of stable passively Q-switched (PQS) operation, which is ascribed to unwanted heating of the SA by the residual (non-absorbed) pump leading to deterioration of its nonlinear properties. According to the stability of Q-switched operation and the pulse characteristics, a low output coupling was selected ($T_{OC} = 3\%$). The PQS laser delivered a stable pulse train up to P_{abs} ~3.5 W. Above this pump level, irregular multi-pulse behavior was observed. The laser output was unpolarized. The laser performance is presented in Fig. 11.

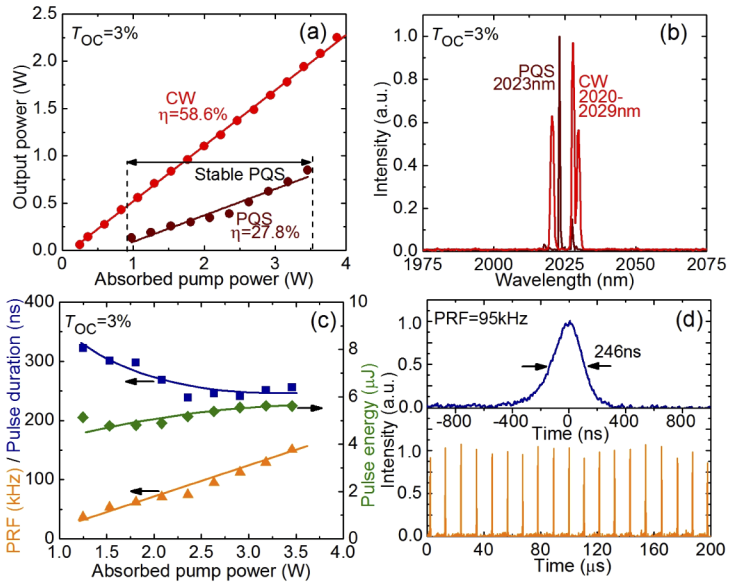

Fig. 11. Diode-pumped SWCNT-SA PQS Tm:$Lu_3Al_5O_{12}$ ceramic laser: (a) input-output dependence, η – slope efficiency; (b) typical laser emission spectrum; (c) pulse duration (FWHM), pulse energy and pulse repetition frequency (PRF) and (d) typical oscilloscope traces of a single Q-switched pulse and the pulse train both measured at $P_{abs} = 2.6$ W and $T_{OC} = 3\%$. (a,b) contain CW regime data for comparison.

The average output power of the PQS laser P_{out} reached 0.85 W at 2023 nm with $\eta = 27.8\%$, Fig. 11(a). With respect to the CW performance, the Q-switching conversion efficiency is reduced to $\eta_{conv} = 43.6\%$. This value is mainly determined by the insertion loss of the SA (Fresnel losses and non-saturable losses of the SWCNT / PMMA film). The laser threshold increased to $P_{abs} = 0.95$ W for the same reason. The laser emission spectrum, Fig. 11(b), became narrower as compared to the CW operation mode, because of the stronger mode competition while bleaching the SA.

The pulse duration (FWHM), $\Delta\tau$, and the pulse repetition frequency (PRF), were measured directly, and the energy of a single Q-switched pulse was calculated as $E_{out} = P_{out}/\text{PRF}$, see Fig. 11(c). The pulse characteristics (duration and energy) were dependent on the pump level which is typical for "fast" SAs such as carbon nanostructures (graphene, SWCNTs) [49]. The latter is explained by the different degree of SA bleaching, which depends on the intracavity intensity. With an increase of the pump power, $\Delta\tau$ shortened from 322 to 256 ns and E_{out} increased from 4.8 to 5.6 μJ. The PRF increased nearly linearly, from 37 to 151 kHz. As a result, the highest peak power $P_{peak} = E_{out}/\Delta\tau$ amounted to 22 W.

A typical oscilloscope trace of a single Q-switched pulse is shown in Fig. 11(d). It has a nearly Gaussian temporal shape, revealing a nearly-optimum ratio between the SA modulation depth

Optics EXPRESS

and the output coupling. The pulse train exhibited relatively weak intensity instabilities, below 15%, as shown in Fig. 11(d). They are attributed to thermal effects in the SA [50].

5. Conclusion

Thulium-doped $Lu_3Al_5O_{12}$ transparent ceramics are promising for continuous-wave, Q-switched and mode-locked lasers at ~2 μm. As compared to their yttrium counterpart, Tm:$Y_3Al_5O_{12}$, they are expected to offer better thermal properties, easier Tm^{3+} doping and advantageous spectroscopic properties (in particular, slightly longer emission wavelength of ~2.02 μm). In the present work, we demonstrated efficient laser operation of a Tm:$Lu_3Al_5O_{12}$ transparent ceramic. A diode-pumped continuous-wave ceramic laser delivered up to 3.12 W at 2022-2035 nm with a slope efficiency of 60.2% (*vs*. the absorbed pump power), which is attributed to the good optical quality of the ceramic and the efficient cross-relaxation for Tm^{3+} ions. Moreover, we characterized the spectroscopic properties of Tm^{3+} in the fabricated $Lu_3Al_5O_{12}$ ceramic. A method to describe correctly the transition intensities from the lower-lying multiplets with $J = 4$ ($^3F_4$) is proposed. For power scaling and improvement of the slope efficiency, it would be promising to fabricate ceramics with even higher Tm doping (>5 at.%) leading to higher pump absorption and more efficient cross-relaxation among Tm^{3+} ions. On the other hand, high doping levels may lead to a decrease of the optical quality and thermal conductivity of ceramics. Thus, a search of an optimum Tm doping is needed. For mode-locked applications, it seems promising to fabricate compositionally "mixed" $(Lu,Y)_3Al_5O_{12}$ ceramics featuring inhomogeneous broadening of the emission spectra.

Funding

Ministerio de Economía y Competitividad (MAT2016-75716-C2-1-R (AEI/FEDER, UE)); Agència de Gestió d'Ajuts Universitaris i de Recerca (2017SGR755); Horizon 2020 Framework Programme (grant agreement No. 739573); European Regional Development Fund (Grant No. CZ.02.1.01/0.0/0.0/15_006/0000674); Ministerstvo Školství, Mládeže a Tělovýchovy (Large Research Infras. Project No. LM2015086, NPU I Project No. LO1602); Chinese Academy of Sciences Key Project (QYZDB-SSW-JSC022).

Acknowledgements

P.L. thanks Dr. Olga Dymshits (St. Petersburg, Russia) for the help with the XRD study.

Disclosures

The authors declare no conflicts of interest.

References

1. A. Ikesue, T. Kinoshita, K. Kamata, and K. Yoshida, "Fabrication and optical properties of high-performance polycrystalline Nd:YAG ceramics for solid-state lasers," J. Am. Ceram. Soc. **78**(4), 1033–1040 (1995).
2. J. Lu, K. I. Ueda, H. Yagi, T. Yanagitani, Y. Akiyama, and A. A. Kaminskii, "Neodymium doped yttrium aluminum garnet (Y3Al5O12) nanocrystalline ceramics – a new generation of solid state laser and optical materials," J. Alloys Compd. **341**(1-2), 220–225 (2002).
3. H. Yagi, T. Yanagitani, K. Takaichi, K. I. Ueda, and A. A. Kaminskii, "Characterizations and laser performances of highly transparent Nd3+:Y3Al5O12 laser ceramics," Opt. Mater. **29**(10), 1258–1262 (2007).
4. A. Ikesue and Y. L. Aung, "Ceramic laser materials," Nat. Photonics **2**(12), 721–727 (2008).
5. J. Lu, M. Prabhu, J. Song, C. Li, J. Xu, K. Ueda, A. A. Kaminskii, H. Yagi, and T. Yanagitani, "Optical properties and highly efficient laser oscillation of Nd:YAG ceramics," Appl. Phys. B **71**(4), 469–473 (2000).
6. K. Takaichi, H. Yagi, J. E. A. Lu, A. Shirakawa, K. Ueda, T. Yanagitani, and A. A. Kaminskii, "Yb3+-doped Y3Al5O12 ceramics – A new solid-state laser material," Phys. Status Solidi A **200**(1), R5–R7 (2003).
7. J. Dong, A. Shirakawa, K. Ueda, H. Yagi, T. Yanagitani, and A. A. Kaminskii, "Laser-diode pumped heavy-doped Yb:YAG ceramic lasers," Opt. Lett. **32**(13), 1890–1892 (2007).

Optics EXPRESS

8. W. X. Zhang, Y. B. Pan, J. Zhou, W. B. Liu, J. Li, B. X. Jiang, X. J. Cheng, and J. Q. Xu, "Diode-pumped Tm:YAG ceramic laser," J. Am. Ceram. Soc. **92**(10), 2434–2437 (2009).
9. H. Chen, D. Shen, J. Zhang, H. Yang, D. Tang, T. Zhao, and X. Yang, "In-band pumped highly efficient Ho:YAG ceramic laser with 21 W output power at 2097nm," Opt. Lett. **36**(9), 1575–1577 (2011).
10. R. Lan, P. Loiko, X. Mateos, Y. Wang, J. Li, Y. Pan, S. Y. Choi, M. H. Kim, F. Rotermund, A. Yasukevich, K. Yumashev, U. Griebner, and V. Petrov, "Passive Q-switching of microchip lasers based on Ho:YAG ceramics," Appl. Opt. **55**(18), 4877–4887 (2016).
11. V. Petrov, "Frequency down-conversion of solid-state laser sources to the mid-infrared spectral range using non-oxide nonlinear crystals," Prog. Quantum Electron. **42**, 1–106 (2015).
12. E. C. Honea, R. J. Beach, S. B. Sutton, J. A. Speth, S. C. Mitchell, J. A. Skidmore, M. A. Emanuel, and S. A. Payne, "115-W Tm:YAG diode-pumped solid-state laser," IEEE J. Quantum Electron. **33**(9), 1592–1600 (1997).
13. R. C. Stoneman and L. Esterowitz, "Efficient, broadly tunable, laser-pumped Tm:YAG and Tm:YSGG cw lasers," Opt. Lett. **15**(9), 486–488 (1990).
14. Z. Pan, Y. Wang, Y. Zhao, H. Yuan, X. Dai, H. Cai, J. E. Bae, S. Y. Choi, F. Rotermund, X. Mateos, J. M. Serres, P. Loiko, U. Griebner, and V. Petrov, "Generation of 84-fs pulses from a mode-locked Tm:CNNGG disordered garnet crystal laser," Photonics Res. **6**(8), 800–804 (2018).
15. Y. Zou, Z. Wei, Q. Wang, M. Zhan, D. Li, Z. Zhang, J. Zhang, and D. Tang, "High-efficiency diode-pumped Tm: YAG ceramic laser," Opt. Mater. **35**(4), 804–806 (2013).
16. Y. Wang, D. Shen, H. Chen, J. Zhang, X. Qin, D. Tang, X. Yang, and T. Zhao, "Highly efficient Tm:YAG ceramic laser resonantly pumped at 1617 nm," Opt. Lett. **36**(23), 4485–4487 (2011).
17. W. L. Gao, J. Ma, G. Q. Xie, J. Zhang, D. W. Luo, H. Yang, D. Y. Tang, J. Ma, P. Yuan, and L. J. Qian, "Highly efficient 2 μm Tm:YAG ceramic laser," Opt. Lett. **37**(6), 1076–1078 (2012).
18. A. Gluth, Y. Wang, V. Petrov, J. Paajaste, S. Suomalainen, A. Härkönen, M. Guina, G. Steinmeyer, X. Mateos, S. Veronesi, M. Tonelli, J. Li, Y. Pan, J. Guo, and U. Griebner, "GaSb-based SESAM mode-locked Tm:YAG ceramic laser at 2 μm," Opt. Express **23**(2), 1361–1369 (2015).
19. Y. Fu, J. Li, C. Wang, T. Xie, W. Li, L. Wu, and Y. Pan, "Fabrication and properties of highly transparent Yb:LuAG ceramics," J. Alloys Compd. **664**, 595–601 (2016).
20. H. Nakao, A. Shirakawa, K. Ueda, H. Yagi, and T. Yanagitani, "CW and mode-locked operation of Yb3+-doped Lu3Al5O12 ceramic laser," Opt. Express **20**(14), 15385–15391 (2012).
21. N. P. Barnes, M. G. Jani, and R. L. Hutcheson, "Diode-pumped, room-temperature Tm:LuAG laser," Appl. Opt. **34**(21), 4290–4294 (1995).
22. K. Scholle, E. Heumann, and G. Huber, "Single mode Tm and Tm,Ho:LuAG lasers for LIDAR applications," Laser Phys. Lett. **1**(6), 285–290 (2004).
23. Y. Wang, R. Lan, X. Mateos, J. Li, C. Li, S. Suomalainen, A. Härkönen, M. Guina, V. Petrov, and U. Griebner, "Thulium doped LuAG ceramics for passively mode locked lasers," Opt. Express **25**(6), 7084–7091 (2017).
24. Z. Zhou, X. Huang, X. Guan, J. Lan, B. Xu, H. Xu, Z. Cai, P. Liu, D. Yan, X. Xu, J. Zhang, M. Lei, and J. Xu, "Continuous-wave and passively Q-switched Tm3+-doped LuAG ceramic lasers," Opt. Mater. Express **7**(9), 3441–3447 (2017).
25. D. Luo, J. Zhang, C. Xu, H. Yang, H. Lin, H. Zhu, and D. Tang, "Yb:LuAG laser ceramics: a promising high power laser gain medium," Opt. Mater. Express **2**(10), 1425–1431 (2012).
26. L. Basyrova, R. Maksimov, V. Shitov, M. Baranov, V. Mikhaylovsky, A. Khubetsov, O. Dymshits, X. Mateos, and P. Loiko, "Effect of SiO2 addition on structural and optical properties of Yb:Lu3Al5O12 transparent ceramics based on laser ablated nanopowders," J. Alloys Compd. **806**, 717–725 (2019).
27. F. Euler and J. A. Bruce, "Oxygen coordinates of compounds with garnet structure," Acta Crystallogr. **19**(6), 971–978 (1965).
28. J. B. Gruber, M. E. Hills, R. M. Macfarlane, C. A. Morrison, G. A. Turner, G. J. Quarles, G. J. Kintz, and L. Esterowitz, "Spectra and energy levels of Tm3+:Y3Al5O12," Phys. Rev. B **40**(14), 9464–9478 (1989).
29. R. D. Shannon, "Revised effective ionic radii and systematic studies of interatomic distances in halides and chalcogenides," Acta Crystallogr. **32**(5), 751–767 (1976).
30. A. A. Kaminskii, H. Rhee, O. Lux, H. J. Eichler, S. N. Bagayev, H. Yagi, K. Ueda, A. Shirakawa, and J. Dong, "Stimulated Raman scattering in "garnet" Lu3Al5O12 ceramics – a novel host-material for Ln-and TM-lasant ions," Laser Phys. Lett. **8**(6), 458–464 (2011).
31. K. Papagelis and S. Ves, "Infrared spectroscopy and lattice dynamical calculations of Gd3Al5O12, Tb3Al5O12 and Lu3Al5O12 single crystals," J. Phys. Chem. Solids **64**(4), 599–605 (2003).
32. Y. Kuwano, K. Suda, N. Ishizawa, and T. Yamada, "Crystal growth and properties of (Lu,Y)3Al5O12," J. Cryst. Growth **260**(1-2), 159–165 (2004).
33. S. A. Payne, L. L. Chase, L. K. Smith, W. L. Kway, and W. F. Krupke, "Infrared cross-section measurements for crystals doped with Er3+, Tm3+, and Ho3+," IEEE J. Quantum Electron. **28**(11), 2619–2630 (1992).
34. B. Aull and H. Jenssen, "Vibronic interactions in Nd:YAG resulting in nonreciprocity of absorption and stimulated emission cross sections," IEEE J. Quantum Electron. **18**(5), 925–930 (1982).
35. C. A. Morrison, E. D. Filer, and N. P. Barnes, "Energy levels and branching ratios of Tm3+ in ten garnet laser materials," report No. HDL-TR-2196, *Harry Diamond Labs Adelphi MD* (1991).
36. B. R. Judd, "Optical absorption intensities of rare-earth ions," Phys. Rev. **127**(3), 750–761 (1962).

Optics EXPRESS

37. G. S. Ofelt, "Intensities of crystal spectra of rare-earth ions," J. Chem. Phys. **37**(3), 511–520 (1962).
38. B. M. Walsh, N. P. Barnes, and B. Di Bartolo, "Branching ratios, cross sections, and radiative lifetimes of rare earth ions in solids: Application to Tm3+ and Ho3+ ions in LiYF4," J. Appl. Phys. **83**(5), 2772–2787 (1998).
39. L. Zhang, H. Lin, G. Zhang, X. Mateos, J. M. Serres, M. Aguiló, F. Díaz, U. Griebner, V. Petrov, Y. Wang, P. Loiko, E. Vilejshikova, K. Yumashev, Z. Lin, and W. Chen, "Crystal growth, optical spectroscopy and laser action of Tm3+-doped monoclinic magnesium tungstate," Opt. Express **25**(4), 3682–3693 (2017).
40. A. A. Kornienko, A. A. Kaminskii, and E. B. Dunina, "Dependence of the line strength of f–f transitions on the manifold energy. II. Analysis of Pr3+ in KPrP4O12," Phys. Status Solidi B **157**(1), 267–273 (1990).
41. P. Loiko, A. Volokitina, X. Mateos, E. Dunina, A. Kornienko, E. Vilejshikova, M. Aguilo, and F. Diaz, "Spectroscopy of Tb3+ ions in monoclinic KLu(WO4)2 crystal: application of an intermediate configuration interaction theory," Opt. Mater. **78**, 495–501 (2018).
42. J. T. Thomas, M. Tonelli, S. Veronesi, E. Cavalli, X. Mateos, V. Petrov, U. Griebner, J. Li, Y. Pan, and J. Guo, "Optical spectroscopy of Tm3+:YAG transparent ceramics," J. Phys. D: Appl. Phys. **46**(37), 375301 (2013).
43. B. J. Fei, J. Q. Huang, W. Guo, Q. F. Huang, J. Chen, F. Tang, W. C. Wang, and Y. G. Cao, "Spectroscopic properties and laser performance of Tm:YAG ceramics," J. Lumin. **142**, 189–195 (2013).
44. W. Jing, P. Loiko, J. M. Serres, Y. Wang, E. Vilejshikova, M. Aguiló, F. Díaz, U. Griebner, H. Huang, V. Petrov, and X. Mateos, "Synthesis, spectroscopy, and efficient laser operation of "mixed" sesquioxide Tm:(Lu,Sc)2O3 transparent ceramics," Opt. Mater. Express **7**(11), 4192–4202 (2017).
45. E. B. Dunina, L. A. Fomicheva, A. A. Kornienko, and M. V. Grigoreva, "Effect of configuration interaction of rare-earth ion states on the intensity of intermultiplet transitions," J. Appl. Spectrosc. **85**(3), 407–415 (2018).
46. P. A. Ryabochkina, S. A. Antoshkina, E. V. Bolshakova, M. A. Ivanov, V. V. Kochurihin, A. V. Malov, S. N. Ushakov, N. V. Shchuchkina, and K. N. Nishchev, "Hypersensitive transitions of Tm3+, Ho3+ and Dy3+ rare-earth ions in garnet crystals," J. Lumin. **132**(8), 1900–1905 (2012).
47. P. Loiko, X. Mateos, S. Y. Choi, F. Rotermund, J. M. Serres, M. Aguiló, F. Díaz, K. Yumashev, U. Griebner, and V. Petrov, "Vibronic thulium laser at 2131 nm Q-switched by single-walled carbon nanotubes," J. Opt. Soc. Am. B **33**(11), D19–D27 (2016).
48. W. B. Cho, A. Schmidt, J. H. Yim, S. Y. Choi, S. Lee, F. Rotermund, U. Griebner, G. Steinmeyer, V. Petrov, X. Mateos, M. C. Pujol, J. J. Carvajal, M. Aguiló, and F. Díaz, "Passive mode-locking of a Tm-doped bulk laser near 2 μm using a carbon nanotube saturable absorber," Opt. Express **17**(13), 11007–11012 (2009).
49. A. S. Yasukevich, P. Loiko, N. V. Gusakova, J. M. Serres, X. Mateos, K. V. Yumashev, N. V. Kuleshov, V. Petrov, U. Griebner, M. Aguiló, and F. Díaz, "Modeling of graphene Q-switched Tm lasers," Opt. Commun. **389**, 15–22 (2017).
50. J. M. Serres, P. Loiko, X. Mateos, K. Yumashev, U. Griebner, V. Petrov, M. Aguiló, and F. Díaz, "Tm:KLu(WO4)2 microchip laser Q-switched by a graphene-based saturable absorber," Opt. Express **23**(11), 14108–14113 (2015).